ARMY RESEARCH LABORATORY

Progress Toward a Multidimensional Representation of the 5.56-mm Interior Ballistics

by John R. Schmidt and Michael J. Nusca

ARL-TR-4903 **August 2009**

NOTICES

Disclaimers

The findings in this report are not to be construed as an official Department of the Army position unless so designated by other authorized documents.

Citation of manufacturer's or trade names does not constitute an official endorsement or approval of the use thereof.

Destroy this report when it is no longer needed. Do not return it to the originator.

Army Research Laboratory
Aberdeen Proving Ground, MD 21005-5066

ARL-TR-4903 **August 2009**

Progress Toward a Multidimensional Representation of the 5.56-mm Interior Ballistics

John R. Schmidt and Michael J. Nusca
Weapons and Materials Research Directorate, ARL

REPORT DOCUMENTATION PAGE	Form Approved OMB No. 0704-0188

1. REPORT DATE *(DD-MM-YYYY)*	2. REPORT TYPE	3. DATES COVERED (From - To)
August 2009	Final	May 2007–September 2008

4. TITLE AND SUBTITLE
Progress Toward a Multidimensional Representation of the 5.56-mm Interior Ballistics

5a. CONTRACT NUMBER

5b. GRANT NUMBER

5c. PROGRAM ELEMENT NUMBER

6. AUTHOR(S)
John R. Schmidt and Michael J. Nusca

5d. PROJECT NUMBER
622618H8000

5e. TASK NUMBER

5f. WORK UNIT NUMBER

7. PERFORMING ORGANIZATION NAME(S) AND ADDRESS(ES)
U.S. Army Research Laboratory
ATTN: RDRL-WMB-D
Aberdeen Proving Ground, MD 21005-5066

8. PERFORMING ORGANIZATION REPORT NUMBER
ARL-TR-4903

9. SPONSORING/MONITORING AGENCY NAME(S) AND ADDRESS(ES)

10. SPONSOR/MONITOR'S ACRONYM(S)

11. SPONSOR/MONITOR'S REPORT NUMBER(S)

12. DISTRIBUTION/AVAILABILITY STATEMENT
Approved for public release; distribution is unlimited.

13. SUPPLEMENTARY NOTES

14. ABSTRACT
There is significant experimental evidence that burning particles of various chemical compositions and sizes are ejected from gun primers and that these particles interact with the propellant grains during main charge ignition. This explicit ignition phenomenon is thought to be incompatible with the implicit treatment of primer function used in conventional interior ballistics codes and models. Generally, the primer efflux is treated as a hot gas that evolves from a specified region in the model's representation of the gun chamber. Essentially, an igniter table is derived from experimental means and by careful calibration of the interior ballistics simulation using gun firing data. With the advent of multidimensional, multiphase interior ballistics codes that employ coupled Eulerian-Lagrangian schemes to explicitly treat both the gas and solid phase, a primer model that is commensurate with the availability of such an interior ballistics model is developed. A further development in the formulation of a primer model that is compatible with the ARL-NGEN3 code and small-caliber weapons is described herein. The model is based on the One-Dimensional Turbulence modeling approach. Integration of the primer model with the ARL-NGEN3 code is shown. Preliminary simulated results comparing primers with particles and primers without particles provide key insights into the early initiation phase of small-caliber ammunition.

15. SUBJECT TERMS
interior ballistics, primer, CFD, two-phase flow, guns

16. SECURITY CLASSIFICATION OF:			17. LIMITATION OF ABSTRACT	18. NUMBER OF PAGES	19a. NAME OF RESPONSIBLE PERSON
a. REPORT	b. ABSTRACT	c. THIS PAGE			John R. Schmidt
Unclassified	Unclassified	Unclassified	UU	34	19b. TELEPHONE NUMBER (*Include area code*) 410-278-5510

Standard Form 298 (Rev. 8/98)
Prescribed by ANSI Std. Z39.18

Contents

List of Figures

Acknowledgments

Program Manager Maneuver Ammunition Systems is gratefully acknowledged for continued support of this effort. Mr. Conroy is acknowledged for many helpful discussions on small-caliber interior ballistics and for acting as a conduit for current information related to this ammunition. Mr. Horst is acknowledged for his assistance in assembling the igniter table representation of the primer.

1. Introduction

Numerical simulation of the interior ballistics (IB) of large-caliber guns has steadily progressed over the last few decades. As a testament to this progress, the U.S. Army Research Laboratory (ARL) (known prior to 1992 as the Ballistics Research Laboratory) has played a major role in the development and popularization of a number of IB codes such as IBHVG2 (*1*), NOVA (also known as XKTC) (*2*, *3*), and NGEN (*4*–*6*), which progress in both model complexity and dimensionality (i.e., zero, one, two, and three dimensions, respectively). A good review of the utility of this suite of IB codes is given by Horst and Nusca (*7*). Through this ambitious and successful progression of IB code development, one area of research that has been paid less attention is the fidelity with which the ignition system (i.e., the primer in small-caliber guns, the primer and flashtube in medium-caliber guns, and the primer and igniter tube in large-caliber guns) is represented. One notable exception is an igniter submodel implemented in the NOVA code for a 105-mm tank gun charge of low vulnerability gun propellant (*8*, *9*). In this model, the primer efflux was treated as gaseous with an added condensing phase that increases the heat transfer coefficient to the propellant.

There is significant evidence that burning particles of various chemical compositions and sizes are ejected from gun primers (*10*–*12*) and interact with the propellant grains during charge ignition. It is perhaps due to this phenomenon that IB code upgrades have had to wait until these same IB codes were made to utilize an explicit, particle-based treatment of the propellant. It would then follow that such an IB code could be made to model the interaction of the discrete primer particles and the discrete propellant particles. With the advent of the ARL-NGEN3 IB code, which employs a coupled Eulerian-Lagrangian scheme to explicitly treat both the continuous (gases) and discrete (solid) phases, the time is ripe for a primer model that is commensurate with the availability of such an IB model.

Such a primer model has been developed; it has been described in previous work (*13*–*15*) and will be summarized in section 2. As a first stage of testing—calibrating and ultimately validating this primer model—the present report describes an effort to couple this model to the multidimensional, multiphase, IB computational fluid dynamics (CFD) code called ARL-NGEN3. The lessons learned will assist in assuring that all the relevant physics have been captured for the purpose of a complete simulation of small-caliber ammunition (see figure 1).

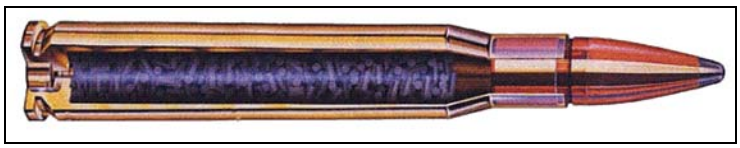

Figure 1. Cutaway of a 5.56-mm small-caliber round.

2. Previous Work

Literature was searched (*13*) to understand the function of the percussion primer and glean the importance and purpose of the ingredients in the no. 41 primer. Overall chemical reactions for the species were derived. NASA-Glen (*16*) thermodynamic calculations were performed as a check of all the major species formed at one atmosphere pressure. Cheetah (*17*) thermodynamics calculations were performed under gun conditions to determine the ideal combustion state for the exploded primer. These conditions are needed for IB calculations. The ideal state was used to estimate physical constants of the gas phase, which were used for the particle-laden One-Dimensional Turbulence (ODT) simulations. It was proposed that the primer could be satisfactorily modeled as a highly turbulent, statistically steady-state, constant density, particle-laden channel flow using one-way coupling. Several different materials came out of the primer tube before the propellant was ignited. The gas phase consisted of the combustion products of lead styphnate, tetracene, pentaerythritoltetranitrate (PETN), and aluminum. The solid phase consisted of the uncombusted barium nitrate and antimony sulfide, which is heated by the hot gases. Thermochemical calculation indicated the presence of a condensed phase as well.

It was found (*13*) that (at least for a first cut) only the drag terms of the particle equation of motion were significant, and particles hitting the wall would stick to the wall rather than bounce off the wall. A channel flow with a bulk Reynolds number (Re) of ~12,000 was chosen to simulate the flow. A brief overview of vector ODT with two-phase flow as it pertains to this application was given. The deposition velocity V_d^+ was calculated for small particle size and compared to literature values for V_d^+. Excellent agreement was achieved for the small radii simulations. A new diameter dependence of V_d^+ was noted. Mean particle velocity profiles across the ODT channel yielded close agreement with measured particle velocities.

Mil spec analysis (*14*) yielded a log-mean diameter of 95 μm for both the antimony sulfide and the barium nitrate. The primer tube was modeled at a steady-state turbulent channel flow with a $Re_\tau = 356$. An analysis of particle behavior across the channel was consistent with trends shown in the literature; the higher the Stokes number, the less sensitive the particles are to wall effects. Particle simulations were performed and converted to R - θ coordinates. Coupling of the ARL-NSRG code (i.e., a general geometry, reacting-flow, multiphase, CFD code) with the statistically steady-state fluid phase velocity profile across the channel was completed in a previous work (*14*). This application was to a clear-chamber ballistic simulator that was used to test fire primers of this type (*18*). The result of this coupled analysis yielded characteristics of a classical underexpended jet into the simulator. Computed results for a series of pressure taps in the simulator are consistent with measurements. An average measured peak pressure of 3 MPa was recorded between 0.03 and 0.04 ms. These simulations showed a peak pressure of 2.6 MPa at 0.04 ms; this was an acceptable agreement, considering the assumptions made. The

experimental data showed a rapid decay of pressure levels to a steady value that was notably lower than the computed value; the computed pressure shows a gradual rise to a steady pressure. The discrepancy between measured and computed results is mostly attributed to the fact that the experiment had heat losses to the surroundings, but the simulation was adiabatic. There is also the probability that there were slight leaks in the experimental apparatus as the ballistic simulators were back to atmospheric pressure shortly after the firings. In the same study, a steady stream of particles was fed into the ARL-NSRG simulation with identical zero initial conditions. The particles were evenly distributed across the opening. Analysis of the initial particle spreading angle yielded a close match to the measured spreading angle of an open-air firing, 72° compared to 70°, respectively. The optical images of the empty ballistic simulator obtained by Williams et al. (*18*) are consistent with the ARL-NSRG simulations.

3. Primer Model and Interface to CFD Code

In order to model the flow from the primer tube into the ammunition chamber, the mean velocity profile for the half-width of the channel (i.e., the primer port), h, was input to the ARL-NGEN3 code for numerical simulation (see figure 2). The mean velocity profile is symmetric around the channel center. The vector ODT model provides instantaneous velocity profiles in the X, Y, and Z directions. The ARL-NGEN3 code uses the axis symmetric coordinate system R, θ, Z. The Z coordinate in the ARL-NSRG code corresponds to the X coordinate in ODT. Hence the streamwise (U) velocity from ODT is the Z velocity for the ARL-NGEN3 code. Since the ARL-NGEN3 code assumes an axis-symmetric velocity profile, the θ velocity component is assumed to be zero. ODT models a one-dimensional line of sight on which the turbulent velocity profile is kept track of in all three dimensions. The θ component in the ARL-NGEN3 code corresponds in this case to the Z component in ODT. The R component in the ARL-NGEN3 code corresponds to the Y component in ODT. The V velocity profile corresponds to the R velocity.

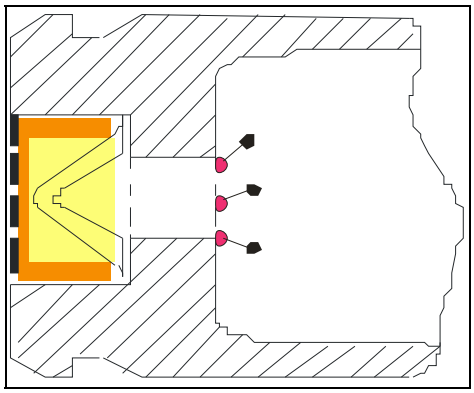

Figure 2. Conceptual drawing of particles inside a 5.56-mm cartridge.

Particles in ODT are allowed to migrate in their own individual space (X, Y, Z) and time (t) line; hence they have their own X, Y, Z, t position. However, all particles are constrained to stay on the ODT one-dimensional domain. Since the particles have their own Y, Z, positions, an attempt was made to map the particle position and velocity into the R, θ coordinates. In the present application, 1260 particles were released and allowed to reach pseudo-steady-state. The particles were binned into 10 equal time increments and converted into R, θ coordinates. The particles in each time bin were sorted to suit the needs of the ARL-NGEN3 code. Particles in the ARL-NGEN3 code must be at least one diameter apart and cannot get within one radius of the walls. The ODT particles in each time bin were sorted in the R coordinate so that they were at a minimum of one radius apart.

4. Modeling Using the ARL-NGEN3 Code

For the present application, the multiphase primer model, described in the previous section, was coupled to the ARL-NGEN3 code. While details of this coupling are provided in the next section, a brief description of this code is included here for completeness. For further details concerning the ARL-NGEN3 code, the reader is referred to papers by Gough (*4*, *19*), Nusca and Gough (*5*), Nusca (*6*, *20*), Nusca and Horst (*7*, *21*), and Schmidt and Nusca (*14*) for both a review of the governing equations and selected code applications.

The Army's NGEN3 code is a multidimensional, multiphase CFD code that incorporates three-dimensional continuum equations and auxiliary relations into a modular code structure. On a sufficiently small scale of resolution in both space and time, the components of the interior ballistic flow are represented by the balance equations for a multicomponent reacting mixture describing the conservation of mass, momentum, and energy. A macroscopic representation of the flow is adopted using these equations derived by a formal averaging technique applied to the microscopic flow. These equations require a number of constitutive laws for closure, including state equations, intergranular stresses, and interphase transfer. The numerical representation of these equations, as well as the numerical solution thereof, is based on a finite-volume discretization and high-order accurate, conservative numerical solution schemes. The spatial values of the dependent variables at each time step are determined by a numerical integration method denoted the Continuum Flow Solver (CFS), which treats the continuous phase and certain discrete phases in an Eulerian fashion. The Flux-Corrected Transport scheme is a suitable basis for the CFS since the method is numerically explicit, computationally robust, and adaptable to massively parallel computer systems. The discrete phases are treated by a Lagrangian formulation, denoted the Large Particle Integrator (LPI), which tracks the particles explicitly and smoothes discontinuities associated with boundaries between propellants yielding a continuous distribution of porosity over the entire domain. The manner of coupling between

the CFS and the LPI is through the attribution of properties (e.g., porosity and mass generation). The size of the grid, as well as the number of Lagrangian particles, is user prescribed. The solid propellant is modeled using Lagrange particles that regress, produce combustion product gases, and respond to gas-dynamic and physical forces. Individual grains, balls, sticks, slab, and wrap layers are not resolved; rather, each propellant medium is distributed within a specified region in the gun chamber. The constitutive laws that describe interphase drag, form-function, etc., assigned to these various media determine preferred gas flow paths through the media (e.g., radial for disks and axial for wraps) and responses of the media to gas-dynamic forces. Media regions that are encased in impermeable boundaries that only yield to gas-dynamic flow after a prescribed pressure load is reached act as rigid bodies within the chamber. Using computational particles to represent the propellant charge permits a host of modeling features that enhance the representation of charge details.

4.1 Overview of the Results

Figure 3 shows a schematic of the computational domain used in the ARL-NGEN3 code for the current simulation of the small-caliber ammunition. Note that figure 3 has the ordinate magnified by about a factor of 7.5 for clarity. In the axial direction, the domain extends from the breech face (X = 0) to the base of the projectile at 4.24 cm (i.e., defined for the present application as the location on the projectile where the diameter matches that of the gun tube near the casemouth); since for this case an axisymmetric configuration is assumed, the domain extends in the radial direction from the centerline to the radial wall of the chamber (0.47 cm maximum radius). The conical afterbody of the ammunition extends back to 3.24 cm (from the breech). The primer resides within the rear wall of the chamber and is modeled using the ARL-NGEN3 code and a variety of techniques that are discussed in detail in this report. The main charge of solid propellant consists of 1.78 g of WC844 deterred ball propellant, the burn rate and thermochemical properties of which are well known. The ARL-NGEN3 code models this region of ball propellant explicitly, using an array of Lagrange particles that are initially ordered but are free to move according to the appropriate governing equations as the simulation proceeds. Each LPI particle has the same size consideration and thermodynamic, mass, and burning properties as the propellant it represents; a certain number of propellant grains are represented by each LPI particle as determined by a number density weighting factor. There are two small regions of empty space or ullage (blue color in the figure) that exist initially within the chamber—one between the primer hole and the rear face of the main charge, beneath the rear chambrage, and the other beneath the forward chambrage. These regions are placed for modeling conveniences since their actual existence is difficult to determine. The black, purple, and green dots located on the radial tube wall mark the location at which wall pressure values are collected as a function of time (see discussions for figure 4) or what can be termed numerical pressure “taps.”

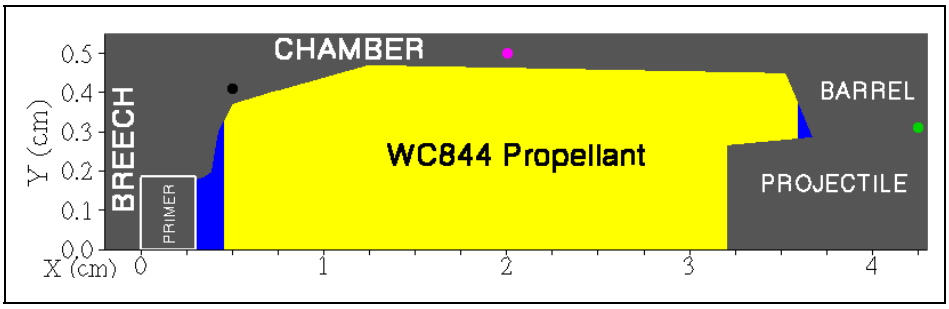

Figure 3. ARL-NGEN3 code setup for small-caliber ammunition simulation.

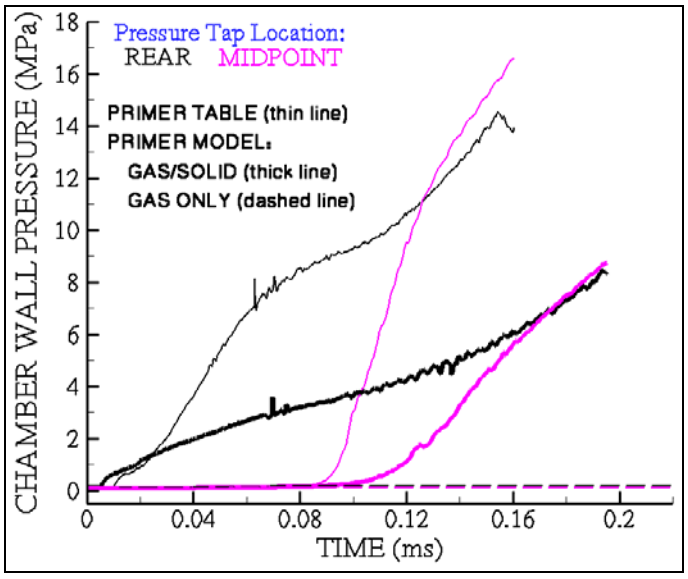

Figure 4. ARL-NGEN3 code results for chamber wall pressures at two axial locations (see figure 3) and for three models of the primer.

Before proceeding to a detailed presentation of the modeling results, an appropriate overview of the present effort is gained from an examination of the computed pressures at the numerical "tap" locations. As mentioned previously, the primer region (recall figure 3) can be represented using three techniques:

1. Assumed Primer Output Table: a table specifying the mass generation, 6700 g/cm^3-s, of hot gases from simulation start to 0.15 ms and over a region bounded by $0 > X > 0.28$ cm, $0 > Y > 0.184$ cm. The specified value of mass generation was computed using known characteristics of the M41 primer performance (0.025 g) and is admittedly larger than thought achievable, and too prompt. Nevertheless, using a table of this kind is well within the conventional practice for modeling small-caliber primers.

2. Multiphase Primer Model: a multiphase (solid and gas) primer model that uses state-of-the-art CFD techniques to compute the gas efflux and solid particle generation of the M41 primer, as described in the previous section and in Schmidt and Nusca (*13*, *14*). This model is coupled to the ARL-NGEN3 code in a one-way fashion (i.e., the primer model is not affected by the ARL-NGEN3 code results) along $0 > Y > 0.184$ cm at $X = 0.38$ cm.

3. Multiphase Primer Model (gas output only): a multiphase primer model employed in the ARL-NGEN3 code by ignoring the generation of solid particles from the primer. This is equivalent to making a speculative or notional primer that is identical to the previously desribed model in all aspects but particles.

Figure 4 shows the computed chamber wall pressures at two of the three locations; the simulations were stopped before the projectile moved to the casemouth position, and thus no data from the third numerical pressure "tap" was obtained. The results generated using the primer output table show a rapid rise in pressure beneath the rear chambrage (i.e., first pressure tap) that reaches about 14 MPa when the primer ceases operation at 0.15 ms. Apparently, flamespreading reaches the mid-chamber point (i.e., second pressure tap) at about 0.09 ms when that region begins to pressurize. Overall, flamespreading through the propellant bed appears to be quite prompt when the primer output table is used. The results generated using the primer model and assuming both gas and solid particle output show a much more gradual pressure rise and a more even pressurization of the propellant bed as evidenced by the equilibration of pressures from both taps to 8 MPa at about 2 ms when the simulation was stopped. When the solid particle output from the primer model is ignored, pressurization of the propellant bed is negligible and indicates a failure to ignite. These results are further explained in section 4.2.

4.2 Detailed Results Using an Assumed Primer Output Table

The detailed results of the ARL-NGEN3 simulation are displayed in figures 5–7 for times of 0.01 to 0.16 ms from start of outflow from the primer region (see figure 3). Note figures 5–7 have the ordinate magnified by about a factor of 7.5 for clarity. In each figure, a particular time is displayed using three computed variables: porosity, propellant temperature, and gas pressure. Selected velocity vectors (in white) are overlaid in each case that displays the magnitude (via vector length) and direction of the local gas field. The porosity (plotted with limits of 0–1: red-blue) of the entire propellant bed is initially about 0.38 (green); the propellant displacement /compression is indicated by a color change to yellow and red while the consumption of propellant is indicated by a color change to light blue. The location of ignited propellant is indicated by colors from green to red (i.e., warm temperature to ignition temperature of 444 K) in the propellant temperature contours. High gas pressure is indicated by the color red with lower pressures indicated by a succession of colors from orange to blue (note that plotted pressure limits of the pressure contours change with each figure).

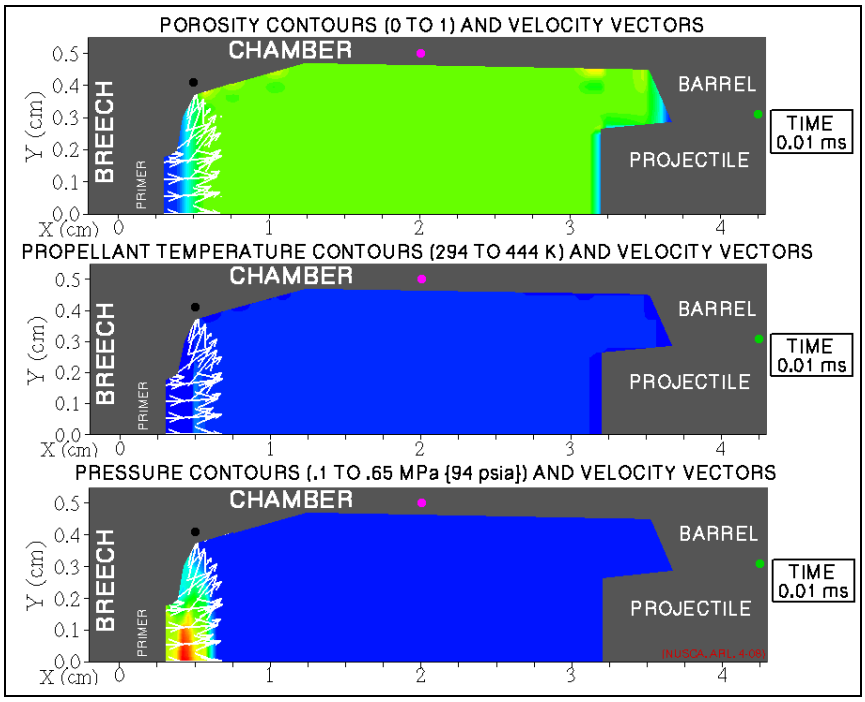

Figure 5. ARL-NGEN3 code results for contours of charge porosity, propellant temperature, and gas pressure with selected velocity vectors; tabular primer output model (time since primer function 0.01 ms).

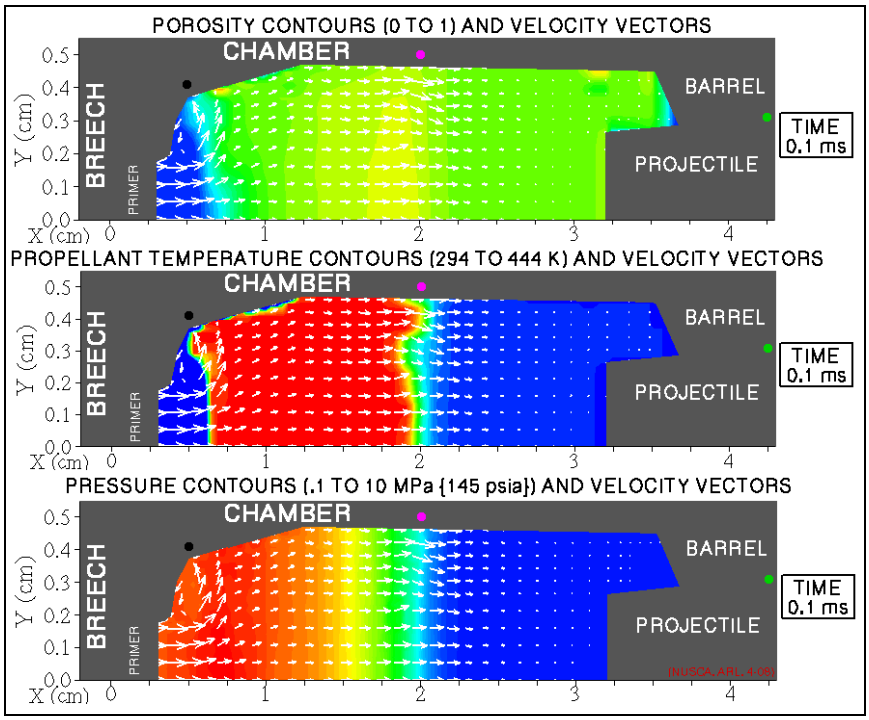

Figure 6. ARL-NGEN3 code results for contours of charge porosity, propellant temperature, and gas pressure with selected velocity vectors; tabular primer output model (time since primer function 0.1 ms).

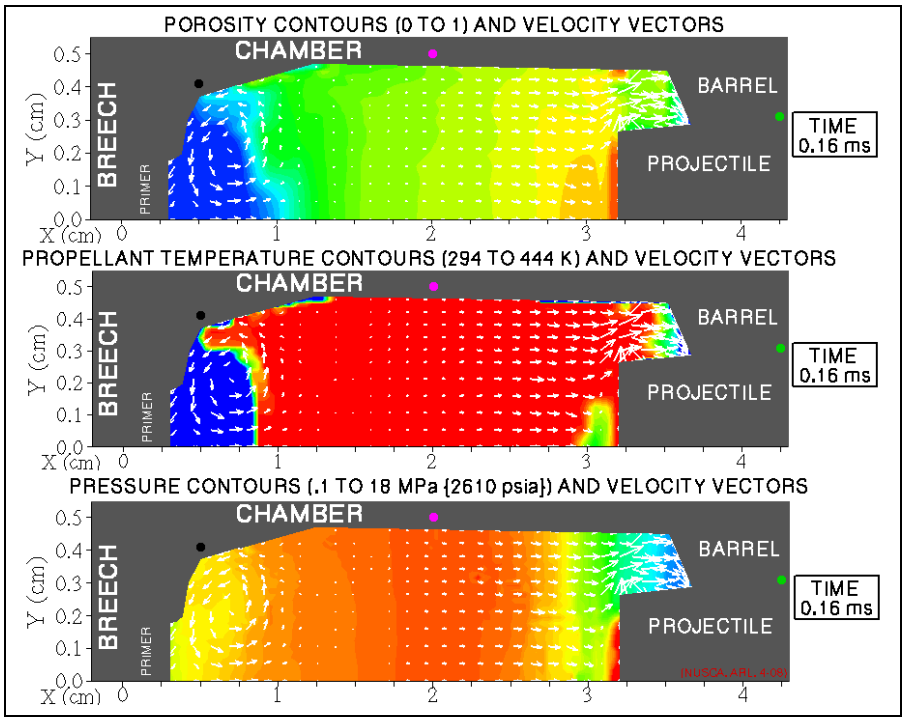

Figure 7. ARL-NGEN3 code results for contours of charge porosity, propellant temperature, and gas pressure with selected velocity vectors; tabular primer output model (time since primer function 0.16 ms).

Figure 5 shows results just past the start of the simulation. The output from the primer table is quite strong, producing an initial supersonic flow velocity of about 400 m/s. The formation of a precursor shock and transitional subsonic flow region or Mach disk (i.e., the localized region of high pressure at the centerline in figure 5) at this early time highlights the brisance of the primer table. The results of figure 6 for a time of 0.1 ms show the formation of a reverse flow region beneath the rear chambrage, the forward displacement and mid-chamber compression of the propellant bed, flamespreading of the propellant to mid-chamber, and the pressurization of the chamber near the breech. At a time right after the ending of the primer table (0.16 ms, as seen in figure 7), the propellant bed, although fully ignited, is notably displaced from the breech and significantly compressed at the base of the projectile afterbody (i.e., red color in the porosity contours). High pressures to over 18 MPa are computed for the mid-chamber and the base of the projectile afterbody. At this point, the projectile has just overcome the starting resistance (i.e., shot start) partly due to gas pressure and partly due to propellant compression. The simulation was stopped by the code that determined regions of local porosity smaller than 0.15, which tends to indicate significant propellant grain fracture and accelerated burning in confined regions of the propellant bed, the physics of which are beyond the scope of the code.

Figure 8 underscores this result in terms of the computed porosity and total pressure local to the base of the projectile afterbody as a function of time. The time axis of the figure has been set to start at about 0.12 ms; previously, neither pressure nor material compression waves had reached

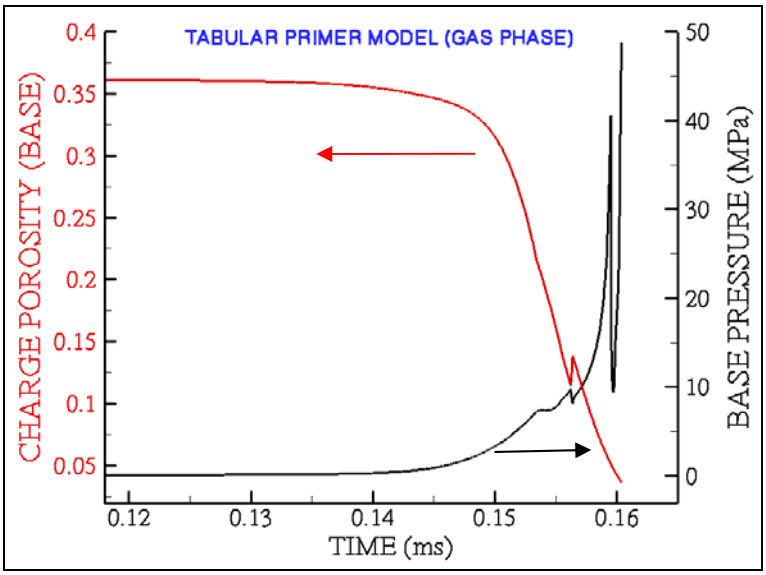

Figure 8. ARL-NGEN3 code results for charge porosity (at the projectile base) and base pressure for the tabular primer output model.

the projectile. Note the rapid drop in local porosity and rise in gas pressure between 0.15 and 0.16 ms. Since the decrease in porosity was so rapid, the code did not halt the simulation until local porosity dropped to an incredible level of 0.03 at which time the base pressure is oscillating. Also note that projectile movement starts at about 0.155 ms as indicated by the transient response in local porosity. As noted previously, the assumed primer output table produces results that appear to be overly severe but do in some ways correspond to dimpling of the projectile base due to propellant compression—a phenomenon that has been observed experimentally.

4.3 Detailed Results Using a Multiphase Primer Model

The detailed results of the ARL-NGEN3 simulation are displayed in figures 9–11 for times of 0.01 to 0.19 ms from start of outflow from the coupled multiphase primer model (see figure 3). Note figures 9–11 have the ordinate magnified by about a factor of 7.5 for clarity. In each figure, a particular time is displayed using three computed variables: porosity, propellant temperature, and gas pressure. Selected velocity vectors (in white) are overlaid in each case that displays the magnitude (via vector length) and direction of the local gas field. The porosity (plotted with limits of 0–1: red-blue) of the entire propellant bed is initially about 0.38 (green); the propellant displacement/compression is indicated by a color change to yellow and red while the consumption of propellant is indicated by a color change to light blue. The location of ignited propellant is indicated by colors from green to red (i.e., warm temperature to ignition temperature of 444 K) in the propellant temperature contours. High gas pressure is indicated by the color red with lower pressures indicated by a succession of colors, orange to blue (note that plotted pressure limits of the pressure contours change with each figure).

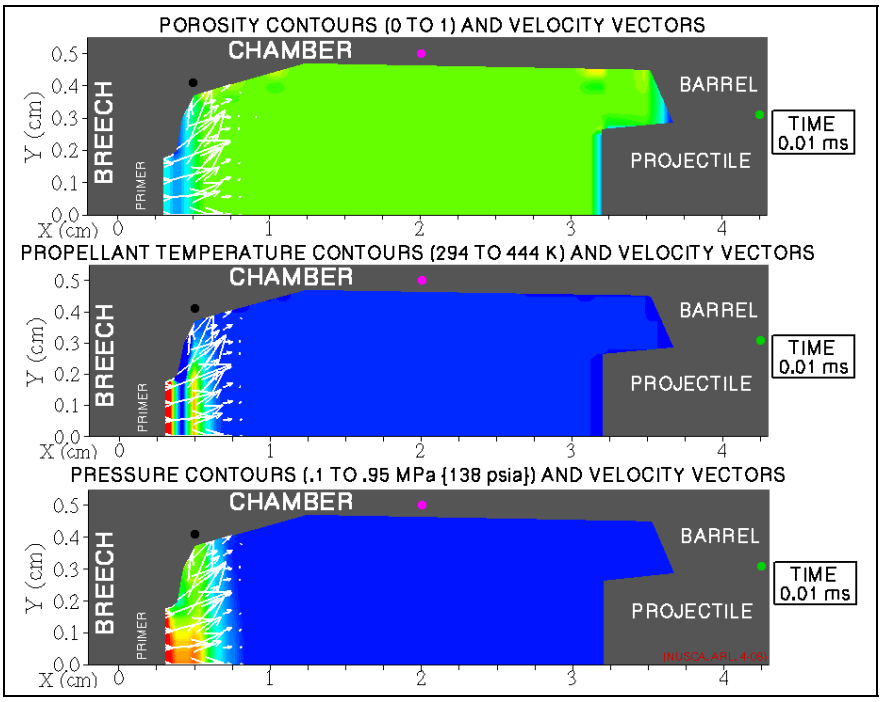

Figure 9. ARL-NGEN3 code results for contours of charge porosity, propellant temperature, and gas pressure with selected velocity vectors; multiphase primer model (time since primer function 0.01 ms).

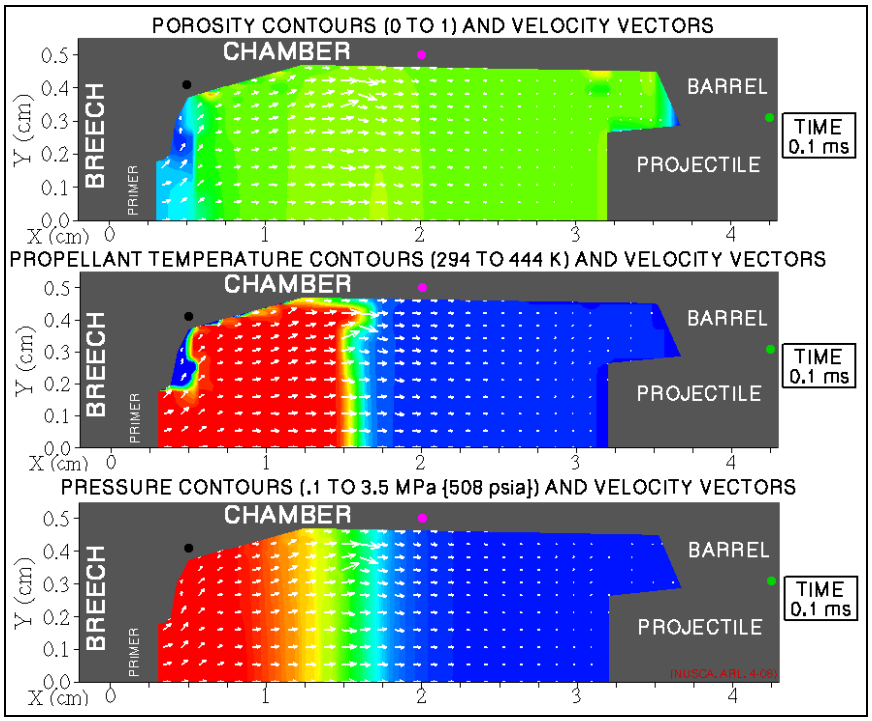

Figure 10. ARL-NGEN3 code results for contours of charge porosity, propellant temperature, and gas pressure with selected velocity vectors; multiphase primer model (time since primer function 0.1 ms).

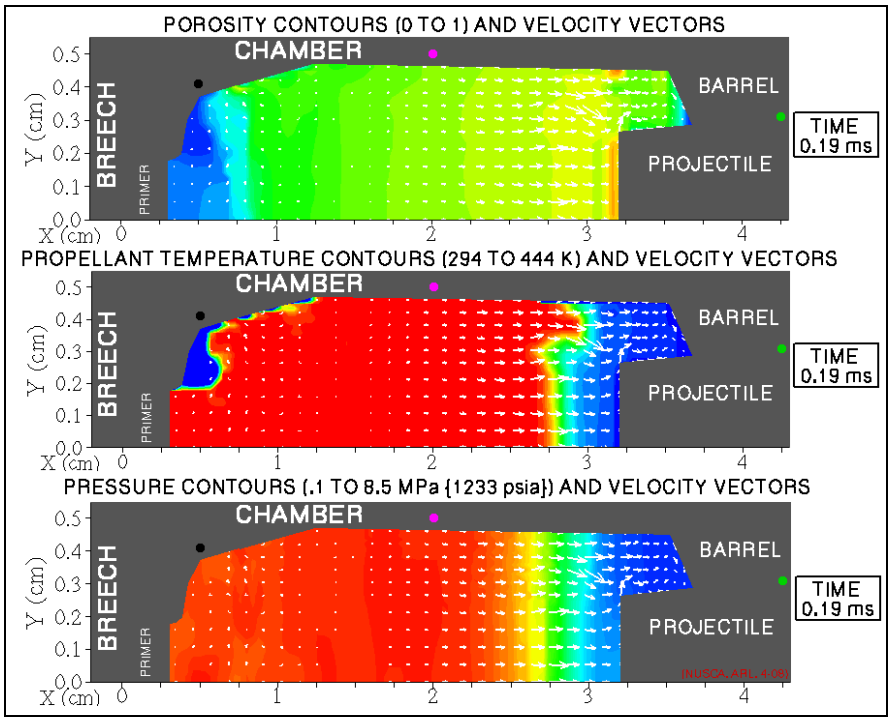

Figure 11. ARL-NGEN3 code results for contours of charge porosity, propellant temperature, and gas pressure with selected velocity vectors; multiphase primer model (time since primer function 0.19 ms).

Figure 9 shows results just past the start of the simulation. The output from the primer table is quite strong, producing an initial supersonic flow velocity of about 90 m/s. The formation of a precursor shock and transitional subsonic flow region or Mach disk (i.e., the localized region of high pressure at the centerline in figure 9) at this early time highlights the strength of the gas flow from the primer model. The results are similar to those of figure 5 with slightly higher local gas pressure (i.e., 0.95 vs. 0.65 MPa) caused by the presence of an ignited solid phase emerging from the primer port (see figure 9 propellant temperature contours). A close comparison of the propellant temperature contour results from the multiphase primer model (figure 9) and the assumed primer table (figure 5) shows that the WC844 propellant bed is actually heated by the primer particle output for the multiphase treatment while still cold for the gas-only treatment. This is a significant result demonstrating for the first time the importance of the particles produced by the primer for the ignition of the main charge.

The results of figure 10 for a time of 0.1 ms show the formation of mild convective flow through the propellant bed, very slight forward displacement and mid-chamber compression of the propellant bed, flamespreading of the propellant to almost mid-chamber, and the pressurization of the chamber near the breech. When compared to the results for the assumed primer output table (figure 6), which show strong convection through the propellant bed, rapid flamespreading, and high chamber pressures, it is clear that flamespreading of the charge in this case is controlled

more by the conduction of heat into the bed caused by the presence of hot particles issuing from the primer port.

By 0.19 ms, as seen in figure 11, the propellant bed is not fully ignited and the chamber is at a pressure level about one-half that produced in the previous simulation (recall figure 7) before the simulation was stopped by the code that determined regions of local porosity smaller than 0.15 (again, indicating significant propellant grain fracture and accelerated burning in confined regions of the propellant bed, the physics of which are beyond the scope of the code). At this time, the propellant bed is notably displaced from the breech and significantly compressed at the base of the projectile afterbody (i.e., yellow and red colors in the porosity contours). Gas pressure at the base of the projectile afterbody is still quite low, but at this point the projectile has just overcome the starting resistance due to localized propellant compression.

Figure 12 underscores this result in terms of the computed porosity and total pressure local to the base of the projectile afterbody as a function of time. The time axis of the figure has been set to start at about 0.13 ms, previous to which neither pressure nor material compression waves have reached the projectile. Note the rapid drop in local porosity and rise in gas pressure between 0.17 and 0.19 ms. Since the decrease in porosity was so rapid, the code did not halt the simulation until local porosity dropped to a level of 0.1 at which time the base pressure is oscillating. Also note that projectile movement starts at about 0.188 ms as indicated by the transient response in local porosity. Although a similar IB result is achieved (i.e., shot start), the details of these results are quite different from those achieved using the assumed primer output table and indicate perhaps the true multiphase nature of ignition and flamespreading in this charge.

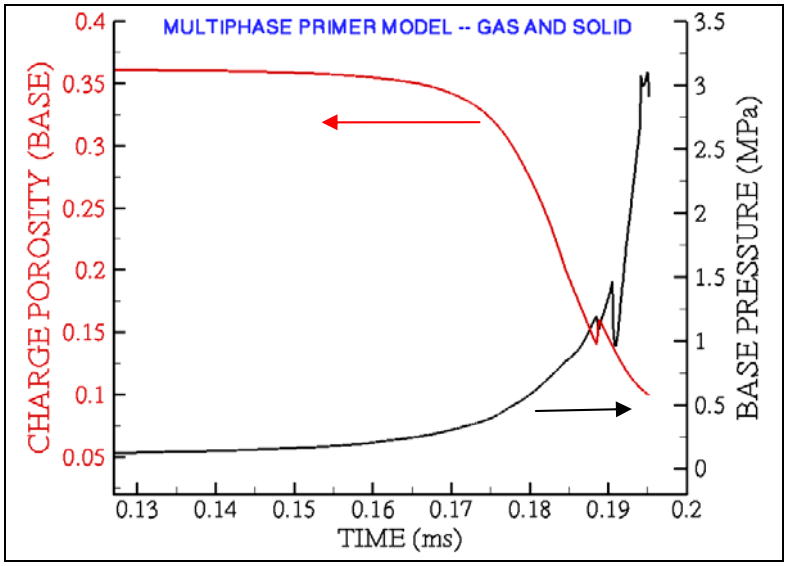

Figure 12. ARL-NGEN3 code results for charge porosity (at the projectile base) and base pressure for the tabular multiphase primer model.

4.4 Detailed Results Using a Multiphase Primer Model—Gas Output Only

The multiphase primer model (gas output only) has the gas phase identical to the multiphase primer model as discussed in section 4.3 but employed in the ARL-NGEN3 code by ignoring the generation of solid particles from the primer. This is equivalent to making a speculative or notional primer that is identical to section 4.3 in all aspects but particles.

The detailed results of the ARL-NGEN3 simulation are displayed in figures 13–15 for times of 0.01 to 1.05 ms from start of gas-only outflow from the coupled primer model (see figure 3). Note figures 13–15 have the ordinate magnified by about a factor of 7.5 for clarity. In each figure, a particular time is displayed using three computed variables: porosity, propellant temperature, and gas pressure. Selected velocity vectors (in white) are overlaid in each case that displays the magnitude (via vector length) and direction of the local gas field. The porosity (plotted with limits of 0-1: red-blue) of the entire propellant bed is initially about 0.38 (green); the propellant displacement/compression is indicated by a color change to yellow and red while the consumption of propellant is indicated by a color change to light blue. The location of ignited propellant is indicated by colors from green to red (i.e., warm temperature to ignition temperature of 444 K) in the propellant temperature contours. High gas pressure is indicated by the color red with lower pressures indicated by a succession of colors from orange to blue (note that plotted pressure limits of the pressure contours change with each figure).

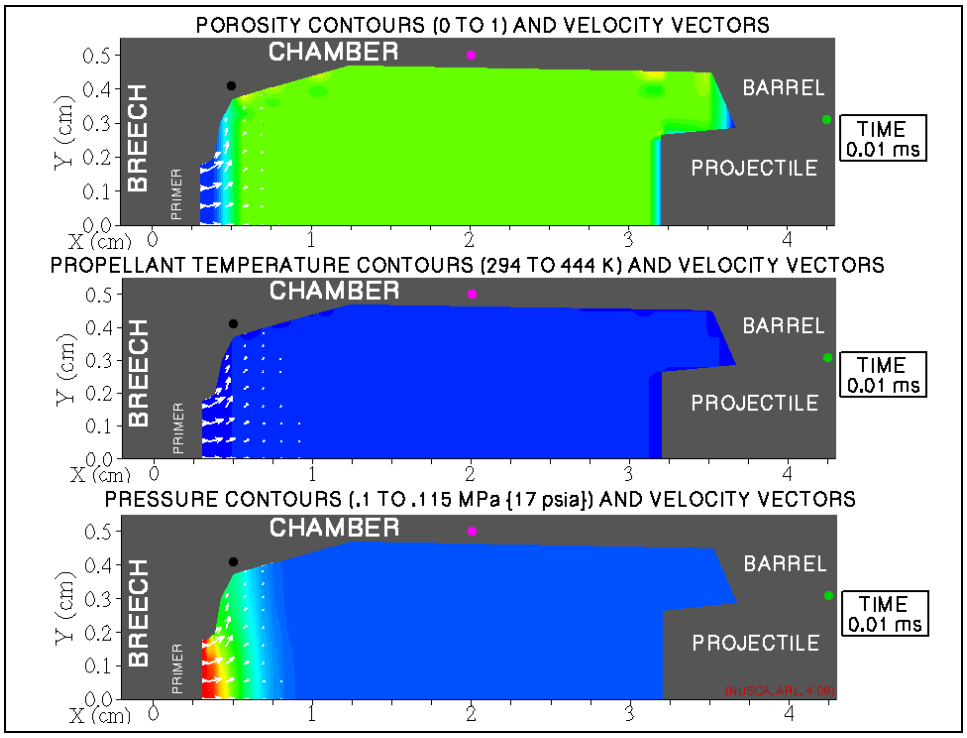

Figure 13. ARL-NGEN3 code results for contours of charge porosity, propellant temperature, and gas pressure with selected velocity vectors; multiphase primer model (gas output only) (time since primer function 0.01 ms).

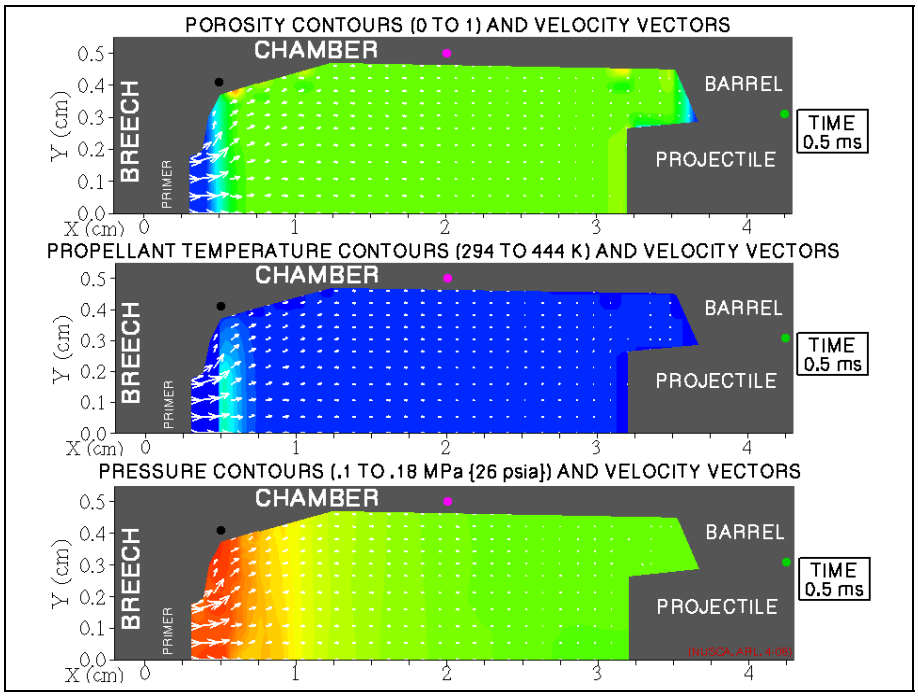

Figure 14. ARL-NGEN3 code results for contours of charge porosity, propellant temperature, and gas pressure with selected velocity vectors; multiphase primer model (gas output only) (time since primer function 0.5 ms).

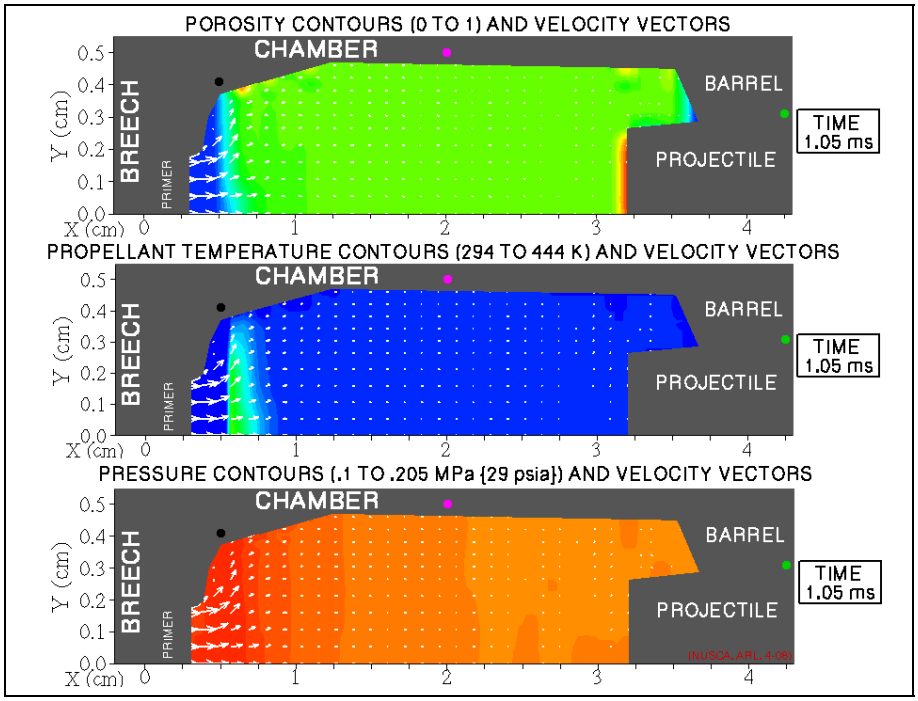

Figure 15. ARL-NGEN3 code results for contours of charge porosity, propellant temperature, and gas pressure with selected velocity vectors; multiphase primer model (gas output only) (time since primer function 1.05 ms).

The results presented in this section serve to isolate the significant effect of the production of hot particles from the primer port by assuming a gas-only output. A sequential viewing of these results in figures 13–15 shows that over an extended time frame (i.e., nearly an order of magnitude longer than the previous results) (1) the propellant bed is slightly displaced from the breech but notably compressed against the projectile base, (2) due to the forward compaction of the propellant bed, there is minimal convective flow though the bed, which causes local heating but no ignition, and (3) pressure levels in the chamber are only about twice ambient. Figure 16 underscores these results in terms of the computed porosity and total pressure local to the base of the projectile afterbody as a function of time. The time axis of the figure has been set to start at about 0.2 ms, previous to which neither pressure nor material compression waves have reached the projectile. Note the gradual drop in local porosity and rise in gas pressure between 0.4 and 1.05 ms. Since the decrease in porosity was so gradual, the code halted the simulation when the local porosity dropped to a level of 0.15. Also note that projectile movement starts at about 0.9 ms as indicated by the transient response in local porosity. Although a similar IB result is achieved (i.e., shot start), the details of these results are quite different from those achieved using the multiphase primer model and indicate the importance of the solid phase to charge ignition for this caliber.

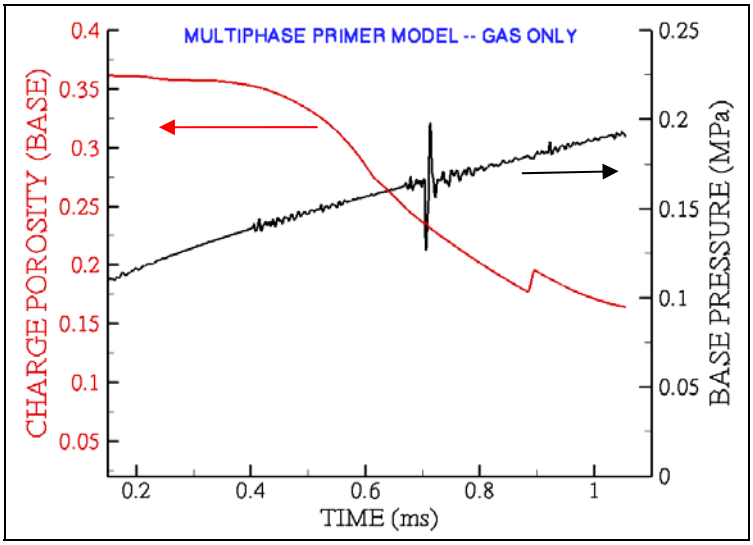

Figure 16. ARL-NGEN3 code results for charge porosity (at the projectile base) and base pressure for the multiphase primer model (gas output only).

4.5 Summary of the Results

Figure 17 shows the results of the three primer modeling techniques for computed propellant bed porosity local to the base of the projectile afterbody replotted from figures 8, 12, and 16. The time axis of the figure has been set to start at about 0.1 ms, previous to which material

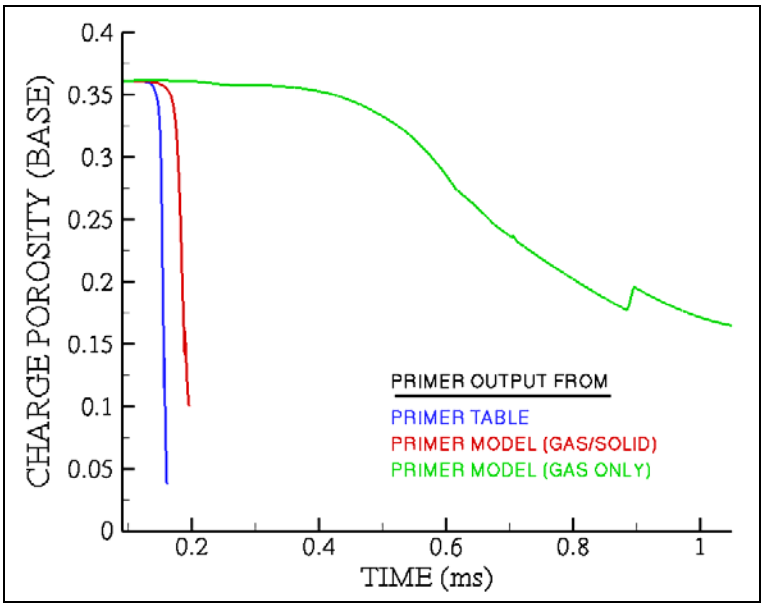

Figure 17. ARL-NGEN3 code results for charge porosity (at the projectile base) using several primer representations.

compression waves have not reached the projectile. All three techniques show an axial compression of the propellant bed in the chamber up to a point of small local porosity (<0.15) and assumed local propellant grain fracture. With the exception of the gas-only primer output derived from the multiphase primer model (i.e., ignoring solid particle production), this compression occurs during ignition and flamespreading of the propellant bed and results in shot start. Shot start occurs due to both gas pressure buildup and the compression of the solid phase at the projectile base. The assumed tabular output from the primer while solely gaseous generates enough brisance to ignite the bed due to convection even when causing the greatest bed compression, i.e., the convective flame outruns the compression wave. Using the combined gas and solid output from the multiphase primer model causes the propellant bed to be heated and ignited by the primer particles; this result is not achievable when the primer particles are ignored since the gas-only output compacts the propellant bed before significant convective flow can cause ignition. Although the compression wave tends to outrun the convective flame, the hot particles conduct heat to the propellant and induce ignition. This is a significant result demonstrating for the first time the importance of the particles produced by the primer for igniting the main charge and has not appeared elsewhere in the literature.

It is important to note that the “gas-only” primer is a notional primer and has a lower temperature and pressure than a no. 41 primer that is allowed to go to completion, such as the primer table shown in section 4.2. This temperature and pressure difference explains why the primer table example ignites the propellant, but the notional gas-only primer does not. The burning particles emitted into the propellant chamber give the added energy needed to ignite the propellant in section 4.3.

5. Conclusions

The latest application of the two-dimensional ARL-NGEN3 model to small-caliber 5.56-mm ammunition has been presented. The code utilizes an explicit treatment of the solid propellant main charge and for the primer both a conventional gas-phase-only treatment and a new physics-based primer submodel. This primer submodel provides two-phase flow characteristics to and is one-way coupled with the ARL-NGEN3 code. The submodel is based on the One-Dimensional Turbulence model, which predicts all relevant velocity scales for both the fluid and the particles based on Reynolds number and Stokes number. This has demonstrated a key point for the physics of small-caliber ammunition. Regions of reverse flow, shot start, and severe propellant bed compaction (which is linked to the dimpling seen experimentally in fired 5.56-mm rounds) are among the many new phenomena revealed using this model. When the conventional gas-phase igniter table was used, as shown in figures 5–8, key points of interest were demonstrated in accordance with expectation. The new igniter submodel, designed to capture the relevant physics as shown in figures 9–12, demonstrated significant differences when compared to the conventional primer treatment. In addition, a notional primer was devised in which the primer produces the same gas output as used in the two-phase model, but no burning particles are included. That is to say, it was a gas-phase-only primer. In the case of this notional primer, the gas-phase igniter was unable to ignite the main charge propellant in the chamber. This is a significant result demonstrating for the first time the importance of the particles produced by the primer for the ignition of the main charge. A sensitivity study using this new submodel coupled to the ARL-NGEN3 code is being considered for future work.

6. References

1. Anderson, R.; Fickie, K. *IBHGV2 – A User's Guide*; BRL-TR-2829; U.S. Army Ballistics Research Laboratory: Aberdeen Proving Ground, MD, July 1987.

2. Gough, P. S. *Interior Ballistics Modeling: Extensions to the XKTC Code and Analytical Studies of Pressure Gradient for Lumped Parameter Codes*; ARL-CR-460; U.S. Army Research Laboratory: Aberdeen Proving Ground, MD, February 2001.

3. Minor, T. C.; Horst, A. W. *Theoretical and Experimental Investigation of Flamespreading Processes in Combustible-Cased Stick Propelling Charges*; BRL-TR-2710; U.S Army Ballistics Research Laboratory: Aberdeen Proving Ground, MD, February 1986.

4. Gough, P. S. Modeling Arbitrarily Packaged Multi-Increment Solid Propellant Charges of Various Propellant Configurations. *Proceedings of the 33rd JANNAF Combustion Meeting*, Monterey, CA, November 1996; CPIA Publication 653, Vol. 1, pp 421–435. (Gough, P. S. *Formulation of a Next-Generation Interior Ballistic Code*; ARL-CR-68; U.S. Army Research Laboratory: Aberdeen Proving Ground, MD, September 1993.)

5. Nusca, M. J.; Gough, P. S. Numerical Model of Multiphase Flows Applied to Solid Propellant Combustion in Gun Systems. AIAA Paper No. 98-3695, July 1998.

6. Nusca, M. J. *High-Performance Computing and Simulation for Advanced Armament Propulsion*; ARL-TR-3215; U.S. Army Research Laboratory: Aberdeen Proving Ground, MD, June 2004.

7. Horst, A. W.; Nusca, M. J. The Charge Designer's Workbench: A Range of Interior Ballistic Modeling Tools. *Proceedings of the 53rd JANNAF Propulsion Meeting*, CPIAC JPMCD05, Monterey, CA, 5–8 December 2005.

8. Gough, P. S. Modeling Chemical Interactions in Ignition of Gun Propellants. *Proceedings of the 22nd JANNAF Combustion Meeting*, Pasadena, CA, October 1983; CPIA Publication No. 432, Vol. 1.

9. Keller, G. E.; Horst, A. W. *The Two Phase Flow Simulation of LOVA Propellant Interior Ballistic Behavior Using the XNOVAK Code*; BRL-TR-2796; U.S. Army Ballistics Research Laboratory: Aberdeen Proving Ground, MD, April 1987.

10. Davis, T. L. *The Chemistry of Powder and Explosives*; Wiley & Sons: New York, 1943.

11. Ekstedt, E. E.; Vest, D. C.; Emerson, V. C.; Dean, L. W. *Pressure Studies of Artillery Primers Fired Statically*; BRL report no. 938; U.S. Army Ballistics Research Laboratory: Aberdeen Proving Ground, MD, June 1955.

12. Chang, L.-M.; Rocchio, J. J. *Simulator Diagnostics of the Early Phase Ignition Phenomena in a 105-mm Tank Gun Chamber*; BRL-TR-2890; U.S. Army Ballistics Research Laboratory: Aberdeen Proving Ground, MD, March 1988.

13. Schmidt, J. R.; Nusca, M. J. Progress in the Development of a Multiphase Turbulent Model of the Gas/Particle Flow in the Primer Tube for Small Caliber Ammunition. *Proceedings of the 53rd JANNAF Propulsion Meeting*, CPIAC JPMCD05, Monterey, CA, December 2005. (See also ARL-TR-3860; U.S. Army Research Laboratory: Aberdeen Proving Ground, MD, August 2006.)

14. Schmidt, J. R.; Nusca, M. J. *Investigation of Small-Caliber Primer Function Using a Multiphase Computational Model*; ARL-TR-4514; U.S. Army Research Laboratory: Aberdeen Proving Ground, MD, July 2008.

15. Schmidt, J. R.; Nusca, M. J. Further Progress on Model Development for Small Caliber Primers. *Proceedings of the 41st JANNAF Combustion Subcommittee Meeting*, San Diego, CA, December 2006.

16. McBride, B. J.; Gordon, S. *Computer Program for Calculation of Complex Chemical Equilibrium Compositions and Applications, II. User's Manual and Program Description*; NASA RP 1311; National Aeronautics and Space Administration: Washington, DC, 1996.

17. Fried, L. E.; Glaesemann, K. R.; Howard, W. M.; Souers, P. C.; Vitello, P. A. Cheetah Code, version 4.0; Lawrence Livermore National Laboratory: Livermore, CA, 2005.

18. Williams, A. W.; Brant, A. L.; Kaste, P. J.; Colburn, J. W. *Experimental Studies of the No. 41 Primer and Ignition of 5.56-mm Ammunition*; ARL-TR-3922; U.S. Army Research Laboratory: Aberdeen Proving Ground, MD, August 2006.

19. Gough, P. S. Extensions to the NGEN Code: Propellant Rheology and Container Properties, October 1997, CPIA Publication 662, Vol. 3, pp 265–281.

20. Nusca, M. J. *Numerical Simulation of the Interior Ballistics for the 105-mm HEP-T M393A3*; ARL-TR-4506; U.S. Army Research Laboratory: Aberdeen Proving Ground, MD, March 2008.

21. Nusca, M. J.; Horst, A. W. *Progress in Modeling Ignition in a Solid Propellant Charge for Telescoped Ammunition*; ARL-TR-3673; U.S. Army Research Laboratory: Aberdeen Proving Ground, MD, November 2005.

NO. OF
COPIES ORGANIZATION

1 (PDF only) DEFENSE TECHNICAL INFORMATION CTR
DTIC OCA
8725 JOHN J KINGMAN RD
STE 0944
FORT BELVOIR VA 22060-6218

1 DIRECTOR
US ARMY RESEARCH LAB
IMNE ALC HRR
2800 POWDER MILL RD
ADELPHI MD 20783-1197

1 DIRECTOR
US ARMY RESEARCH LAB
RDRL CIM L
2800 POWDER MILL RD
ADELPHI MD 20783-1197

1 DIRECTOR
US ARMY RESEARCH LAB
RDRL CIM P
2800 POWDER MILL RD
ADELPHI MD 20783-1197

ABERDEEN PROVING GROUND

1 DIR USARL
RDRL CIM G (BLDG 4600)

NO. OF COPIES	ORGANIZATION
3	DIRECTOR US ARMY RESEARCH LAB AMSRD ARL RO P D MANN R ANTHENIEN TECH LIB PO BOX 12211 RESEARCH TRIANGLE PARK NC 27709-2211
8	US ARMY AVIATN & MSLE CMND AMSRD AMR PS PT W CHEW C DOLBEER J LILLY M LYON J FISHER B MARSH R MICHAELS D THOMPSON REDSTONE ARSENAL AL 35898-5249
4	PM MAS SFAE AMO MAS M BUTLER F HANZL P RIGGS G DEROSA BLDG 354 PICATINNY ARSENAL NJ 07806-5000
8	DIR BENET WEAPONS LAB M AUDINO R DILLON R FISCELLA R HASENBEIN E KATHE K MINER S SOPOK J MCNEIL WATERVLIET NY 12189-4000
1	COMMANDER RADFORD ARMY AMMO PLANT SMCAR QA HI LIB RADFORD VA 24141-0298
1	COMMANDANT USAFC&S ATSF CN P GROSS FORT SILL OK 73503-5600

NO. OF COPIES	ORGANIZATION
5	COMMANDER US ARMY ARDEC C ADAM S EINSTEIN P HUI J O'REILLY J SHIN BLDG 382 PICATINNY ARSENAL NJ 07806-5000
2	COMMANDER US ARMY ARDEC R CARR J MIDDLETON BLDG 65N PICATINNY ARSENAL NJ 07806-5000
2	COMMANDER US ARMY ARDEC R CIRINCIONE J RUTKOWSKI BLDG 171M PICATINNY ARSENAL NJ 07806-5000
1	COMMANDER US ARMY ARDEC J LANNON BLDG 1 PICATINNY ARSENAL NJ 07806-5000
2	COMMANDER US ARMY ARDEC E LOGSDEN S NICOLICH BLDG 65S PICATINNY ARSENAL NJ 07806-5000
1	COMMANDER US ARMY ARDEC B MACHAK BLDG B1 PICATINNY ARSENAL NJ 07806-5000
1	COMMANDER US ARMY ARDEC P O'REILLY BLDG 407 PICATINNY ARSENAL NJ 07806-5000
1	COMMANDER US ARMY ARDEC A SABASTO BLDG 94 PICATINNY ARSENAL NJ 07806-5000

NO. OF COPIES ORGANIZATION

1 COMMANDER
US ARMY ARDEC
R SURAPANENI
BLDG 3022
PICATINNY ARSENAL NJ 07806-5000

2 CDR NVL RSRCH LAB
TECH LIB
J BORIS
WASHINGTON DC 20375-5000

1 OFFICE OF NVL RSRCH
J GOLDWASSER
875 N RANDOLPH ST RM 653
ARLINGTON VA 22203-1927

3 COMMANDER
NAWC
A ATWOOD
S BLASHILL
T PARR
CH1NA LAKE CA 93555-6001

1 AIR FORCE RSRCH LAB
MNME EN MAT BR
B WILSON
2306 PERIMETER RD
EGLIN AFB FL 32542-5910

1 AIR FORCE OFC OF SCI RSRCH
M BERMAN
875 N RANDOLPH ST
STE 235 RM 3112
ARLINGTON VA 22203-1768

1 NASA LANGLEY RSRCH CTR
D BUSHNELL
MS 110
HAMPTON VA 23681-2199

1 DIR SANDIA NATL LABS
M BAER DEPT 1512
PO BOX 5800
ALBUQUERQUE NM 87185

2 DIR LAWRENCE LIVERMORE NL
L FRIED
M MURPHY
PO BOX 808
LIVERMORE CA 94550-0622

NO. OF COPIES ORGANIZATION

1 CENTRAL INTLGNC AGCY
J BACKOFEN
RM 4PO7 NHB
WASHINGTON DC 20505

1 BATTELLE EAST SCI & TECH
A ELLIS
1204 TECHNOLOGY DR
ABERDEEN MD 21001-1228

2 JHU CHEM PROP INFO AGCY
W HUFFERD
R FRY
10630 LITTLE PATUXENT PKWY
STE 202
COLUMBIA MD 21044-3200

1 (CD only) OUSD (AT&L)/STRAT & TACT
SYS MUNITIONS
T MELITA
3090 DEFENSE PENTAGON
RM 3B1060
WASHINGTON DC 20301-3090

1 BRIGHAM YOUNG UNIV
DEPT OF CHEMICAL ENGRG
M BECKSTEAD
PROVO UT 84601

1 CALIF INST OF TECHLGY
F E C CULICK
204 KARMAN LAB
MS 301 46
1201 E CALIFORNIA ST
PASADENA CA 91109

2 UNIV OF ILLINOIS
DEPT OF MECH INDUSTRY ENGRNG
H KRIER
R BEDDINI
144 MEB 1206 N GREEN ST
URBANA IL 61801-2978

5 PENNSYLVANIA STATE UNIV
DEPT OF MECHL ENGRG
K KUO
T LITZINGER
G SETTLES
S THYNELL
V YANG
UNIVERSITY PARK PA 16802-7501

NO. OF
COPIES ORGANIZATION

1 ARROW TECHLGY ASSOC INC
1233 SHELBURNE RD D 8
SOUTH BURUNGTON VT 05403

3 ATK AMMO & ENERGETICS
RADFORD ARMY AMMO PLANT
D WORRELL
W WORRELL
S RITCHIE
RTE 114 PO BOX 1
RADFORD VA 24143

1 ALLEGHENY BALLISTICS LAB
PO BOX 210
ROCKET CENTER WV 26726

1 ATK ORDNANCE
4700 NATHAN LN
PLYMOUTH MN 55442

4 ATK THIOKOL
P BRAITHWAITE
T FARABAUGH
W WALKUP
R WARDLE
PO BOX 707
BRIGHAM CITY UT 84302-0707

1 ATK ELKTON
J HARTWELL
PO BOX 241
ELKTON MD 21921-0241

1 BAE ARMAMENT SYS DIV
JAHN DYVIK
4800 EAST RIVER RD
MINNEAPOLIS MN 55421-1498

1 GEN DYNAMICS ST MARKS
H RAINES
PO BOX 222
SAINT MARKS FL 32355-0222

1 GEN DYNAMICS ARM SYS
J TALLEY
128 LAKESIDE AVE
BURLINGTON VT 05401

3 VERITAY TECHLGY INC
R SALIZONI
J BARNES
E FISHER
4845 MILLERSPORT HWY
EAST AMHERST NY 14501-0305

NO. OF
COPIES ORGANIZATION

ABERDEEN PROVING GROUND

51 DIR USARL
RDRL WM
P PLOSTINS
RDRL WMB
J NEWILL
M ZOLTOSKI
RDRL WMB A
G BROWN
B DAVIS
D HEPNER
G KATULKA
D LYON
RDRL WMB C
P WEINACHT
S SILTON
G COOPER
J DESPIRITO
J GARNER
J SAHU
RDRL WMB D
C CANDLAND
J MORRIS
W ANDERSON
R BEYER
A BRANT
S BUNTE
L CHANG
J COLBURN
P CONROY
B FORCH
B HOMAN
A HORST
S HOWARD
P KASTE
A KOTLAR
R LIEB
K MCNESBY
M MCQUAID
A MIZIOLEK
M NUSCA (5 CPS)
R PESCE-RODRIGUEZ
S PIRIANO
B RICE
R SAUSA
E SCHMIDT
J SCHMIDT (3 CPS)
A WILLIAMS
RDRL WMM
S MCKNIGHT
RDRL WMS
T ROSENBERGER

NO. OF
COPIES ORGANIZATION

RDRL WMT
P BAKER
W CIEPIELA

INTENTIONALLY LEFT BLANK.